Author/s:
Syed, N;Zavabeti, A;Mohiuddin, M;Zhang, B;Wang, Y;Datta, RS;Atkin, P;Carey, BJ;Tan, C;van Embden, J;Chesman, ASR;Ou, JZ;Daeneke, T;Kalantar-zadeh, K

Title:
Sonication-Assisted Synthesis of Gallium Oxide Suspensions Featuring Trap State Absorption: Test of Photochemistry

Date:
2017-11-17

Citation:
Syed, N., Zavabeti, A., Mohiuddin, M., Zhang, B., Wang, Y., Datta, R. S., Atkin, P., Carey, B. J., Tan, C., van Embden, J., Chesman, A. S. R., Ou, J. Z., Daeneke, T. & Kalantar-zadeh, K. (2017). Sonication-Assisted Synthesis of Gallium Oxide Suspensions Featuring Trap State Absorption: Test of Photochemistry. Advanced Functional Materials, 27 (43), https://doi.org/10.1002/adfm.201702295.

DOI: 10.1002/ ((please add manuscript number))

Article type: Full Paper

Sonication-Assisted Synthesis of Gallium Oxide Suspensions Featuring Trap State Absorption: Test of Photochemistry

*Nitu Syed, Ali Zavabeti, Md Mohiuddin, Baoyue Zhang, Yichao Wang, Robi S. Datta, Paul Atkin, Benjamin J. Carey, Cheng Tan, Joel van Embden, Anthony S. R. Chesman , Jian Zhen Ou, Torben Daeneke, Kourosh Kalantar-zadeh**

N. Syed, A. Zavabeti, M. Mohiuddin, B. Zhang, R. S. Datta, P. Atkin, B. J. Carey, Dr. J. Z. Ou, Dr. T. Daeneke, Prof. K. Kalantar-zadeh

School of Engineering, RMIT University, Melbourne, VIC 3000, Australia

E-mail: kourosh.kalantar@rmit.edu.au

Dr. Y. Wang

School of Life and Environmental Sciences, Deakin University, Geelong, Victoria 3216, Australia

C. Tan,Dr J. van Embden

School of Applied Sciences, RMIT University, Melbourne, Victoria 3000, Australia

Dr. A. S. R. Chesman, B. J. Carey,

Manufacturing Business Unit, CSIRO, Clayton, Victoria, 3168 Australia

Keywords: Liquid metal, gallium, trap states, sonication, metal oxide

Gallium is a near room temperature liquid metal with extraordinary properties that partly originate from the self-limiting oxide layer formed on its surface. Taking advantage of the surface gallium oxide, this work introduces a novel technique to synthesize gallium oxide (Ga_2O_3) nanoflakes at high yield by harvesting the self-limiting native surface oxide of gallium. The synthesis process follows a facile two-step method comprising liquid gallium metal sonication in DI water and subsequent annealing. In order to explore the functionalities of the product, the obtained hexagonal α-Ga_2O_3 nanoflakes are used as a photocatalytic material to decompose organic model dyes. Excellent photocatalytic activity is observed under solar light irradiation. To elucidate the origin of these enhanced catalytic properties, we carefully assess the electronic band structure of the synthesized α-Ga_2O_3. Consequently, this excellent photocatalytic performance is associated with an energy band gap reduction, due to the presence of trap states, which are located at ~1.65 eV under the conduction band minimum. This work presents a novel route for synthesizing oxide nanostructures that can be extended to other low melting temperature metals and their alloys, with great prospects for scaling up and high yield synthesis.

1. Introduction

Group III–VI semiconductor gallium (III) oxide (Ga_2O_3) is a promising inorganic compound that crystallizes in five different phases including α, β, γ, δ, and ε.[1] Of these polymorphs, α-Ga_2O_3 and β-Ga_2O_3 are the most investigated.[2] Non-toxic and stable Ga_2O_3 has a wide energy band gap (Eg ≈ 4.2 - 4.9 eV) in its intrinsic form.[2a, 3] This oxide offers great possibilities for a wide range of applications such as optoelectronics,[4] electronic devices,[5] solar cells,[6] gas sensing[7] and more recently, in photocatalysis.[8]

With growing global attention concerning environmental remediation, the exploration and implementation of various photocatalysts has attracted significant interest for decomposing various organic pollutants.[9] However, inefficient absorption of the solar light spectrum, together with rapid deactivation of photocatalysts, limit the practical applications of many of them.[10] It has been shown that Ga_2O_3, despite its relatively wide bandgap, exhibits acceptable photocatalytic performance to decompose different pollutants or organic dyes under UV and visible light irradiation at different phases, stoichiometries and morphologies.[1, 3a, 11] Under optimized conditions, Ga_2O_3 has been shown to have a better photocatalytic performance in comparison to commercial TiO_2 particles, due to its ability to provide photo-generated charge carriers with more suitable redox potentials, leading to higher driving forces for photocatlysis.[12] However, there are still serious limitations for the application of Ga_2O_3 as a photocatalyst due to its wide band gap. Hence, any improvement of the photocatalytic activity of Ga_2O_3 by shifting its photo-response towards the visible range will create a profound positive impact.

Many methods have been investigated to overcome the constraints of photocatalytic activities of Ga_2O_3 including doping, inducing oxygen deficiency and hybridization.[11d, 11e, 13] Nevertheless, none of the studies have shown full evidence regarding the changes that occur on the electronic band

structure of the modified gallium oxides. A fundamental analysis, establishing a relation between the tuned energy band gap of Ga_2O_3 and resulting photocatalytic activity, has been rarely presented.

The choice of synthesis techniques has a profound impact on morphologies, phases and stoichiometries of Ga_2O_3 and therefore its band structure.[14] Many different liquid phase methods have been shown for synthesizing Ga_2O_3 based on hydrothermal (with and without surfactant), microwave and other solvothermal approaches.[1, 2b, 3a, 15] These methods have been reported to result in nanorods, nanowires or nanoplates of various dimensions of this metal oxide. However, such synthesis techniques generally require long processing time of up to several days for acceptable synthesis yields.

Very recently, liquid metal gallium has drawn attention for synthesizing various gallium compounds based on printing processes.[16] The reported methods generally take advantage of the formation of the self-limiting oxide layer on the surface of liquid gallium at room temperature, utilizing techniques to isolate this layer from the original liquid source. The self-limiting gallium oxide layer grows slowly and may become thicker upon environmental excitations and applied mechanic energy.[17]

The existence of the oxide skin on liquid gallium can also provide an opportunity to develop a high yield method for synthesizing Ga_2O_3 nanostructures. It is hypothesized that vigorous sonication and the application of shear forces should assist in removing the oxide layer. Since this oxide is gradually formed on the surface of the metal, which constitutes a reducing metallic environment underneath, it can potentially feature high densities of oxygen vacancies. We hypothesize that these oxygen

vacancies can aid photocatalysis by reducing the bandgap of Ga_2O_3 due to the introduction of trap states, allowing the system to operate in the visible region of the solar spectrum.

Herein we investigate the possibility of using the self-limiting oxide skin of liquid gallium as a precursor for synthesizing suspensions of Ga_2O_3 nanoparticles. A novel two-step synthesis method is demonstrated, leading to gallium oxide nanoflakes and rods, relying on sonicating liquid gallium and annealing the detached native oxide skin. We report on the strong dye degradation performance of the synthesized Ga_2O_3 nanoparticles and characterize the electronic structure of the material, associating enhanced photocatalytic activity to the formation of a trap bands. In our work, we provide a fundamental analysis of the modified energy band structure that is responsible for the high photocatalytic performance of Ga_2O_3 nanostructures.

2. Results and Discussion

As discussed in the Experimental Section, the synthesis was carried out in a two-step process consisting of liquid gallium sonication in DI water followed by annealing, allowing to obtain gallium oxide nanoparticles.

During the sonication step, a gallium metal droplet (**Figure 1**a) splits into micro-to nano-sized spherical or quasi-spherical liquid metal structures (Figure 1b). A self-limiting thin oxide layer grows on the surface of these liquid metal droplets, with the oxide layer becoming thicker during mechanical agitation. The thickening oxide film is expected to crack it into smaller pieces with

increasing sonication duration. The cracked oxide layers are gradually detached from the gallium surface (Figure 1c) to form suspended oxide nanoflakes. Simultaneously, a new self-limiting oxide layer is established on these gallium metal droplets each time an oxide piece departs their surfaces. The breakdown of the liquid metal into smaller droplets and the detachment of oxide flakes from the surface of the metallic gallium is a repetitive process. Thus, the fraction of these nanoplatelets suspended in DI water increases with longer sonication periods. The size of the droplets becomes smaller with sonication time and their number increases. This process continues until the bulk of the liquid gallium is transformed into nanoflakes. A reaction time of 60 min was found to be sufficient to transform the majority of the liquid bulk into oxide nanoparticles. Near the end of the sonication process, the residual larger particles and any remaining metal are removed from the suspended nanoflakes *via* centrifugation (Figure 1d).

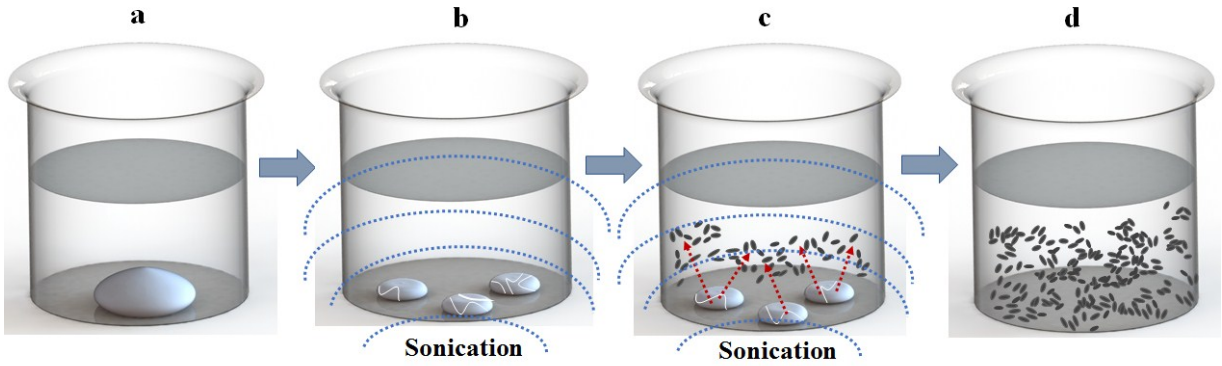

Figure 1. Step-by-step schematic of the synthesis process converting gallium metal into gallium oxide nanoparticles during sonication. (a) A bulk gallium droplet with surface oxide, kept in DI water. (b) The bulk gallium metal splits into smaller liquid metal entities with cracks on their surface oxide skin during sonication. (c) Delamination of small oxide nanoparticles from the cracked surface oxide

layer. (d) Oxide nanoparticles separated from the bulk gallium metal after completed reaction and centrifugation.

Figure 2a-b show the bulk liquid metal droplet in DI water before sonication and the suspension of hydrated oxide nanoparticles after the morphological transformation due to ultrasonic agitation. Figure 2c shows the re-suspended final product after centrifugation and annealing. The slight grey coloration of the final product might be due to residual metallic impurities. If present, however, these impurities should be of very small concentration as they were not encountered during extensive scanning electron microscopy (SEM) and transmission electron microscopy (TEM) imaging and were below the detection limit of X-ray photoelectron spectroscopy (XPS) analysis, which will be discussed later on.

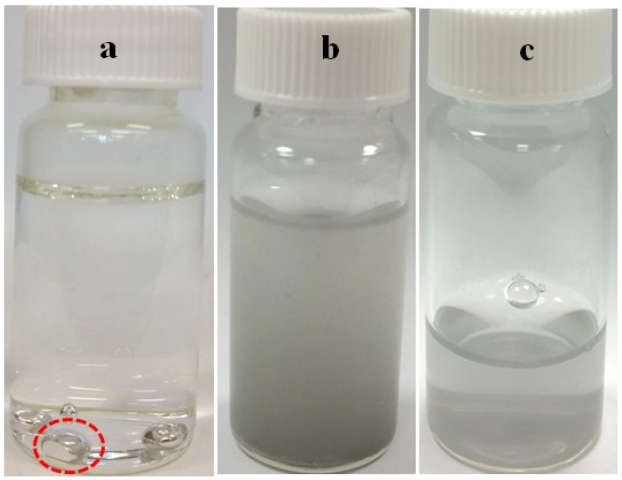

Figure 2. (a) Bulk gallium droplets in DI water. (b) Suspension of hydrated oxide nanoparticles prepared after 60 min of sonication prior to centrifugation. (c) Gallium oxide suspension after centrifugation, annealing and re-suspension.

X-ray diffraction (XRD) was utilized to characterize the crystal phase and crystallinity of the resulting product. **Figure 3**a shows a typical XRD pattern of the suspended nanoparticles after sonication. The diffraction peak positions in the pattern can be clearly indexed to the orthorhombic structure of GaOOH with lattice constants of a = 4.58 Å, b = 9.80 Å, c = 2.97 Å.[18]

The XRD pattern of the obtained powder after annealing was also obtained. The observed diffraction peaks occur at new locations (Figure 3b), indicating that the GaOOH was entirely converted into α-Ga_2O_3. All of the observed diffraction peaks are in good agreement with the reported values for hexagonal α-Ga_2O_3 with lattice constants a = b=4.97 Å, c = 13.42 Å.[18-19] All diffraction peaks could be indexed to α-Ga_2O_3 and no additional diffraction peaks of possible impurities were detected.

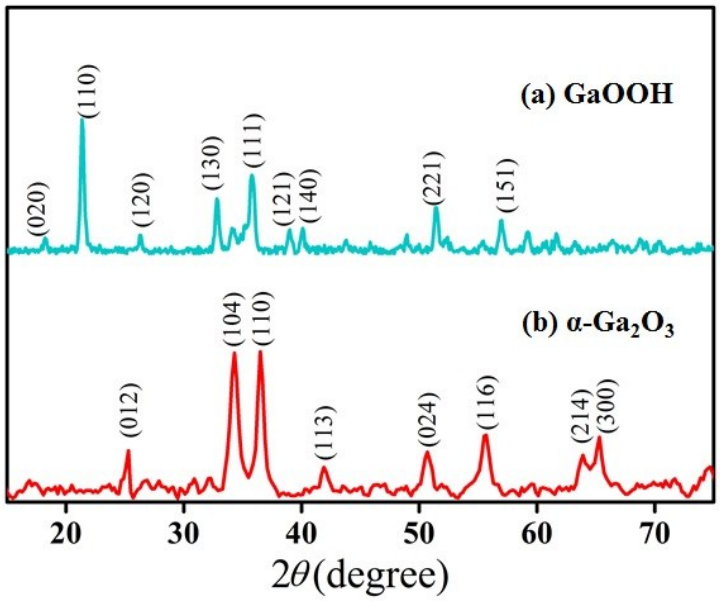

Figure 3. XRD data of (a) as synthesized nanoflakes indexed to GaOOH and (b) annealed material indexed to α-Ga_2O_3.

Scanning and transmission electron microscopy images and selected area electron diffraction (SAED) patterns were obtained for further morphological and structural analysis of the GaOOH and Ga_2O_3 particles. The obtained data for the intermediate product GaOOH is presented in Supporting Information (Figure S1, Supporting Information). GaOOH nanoparticles were found to display a plate-like non-porous morphology.

Figure 4a-b depict the SEM images of the final product after annealing, revealing that the sizes of the α-Ga_2O_3 nanoflakes are not uniform and that the nanoflakes consist of two types of structures. The most commonly observed structures are plates of 25-250 nm widths and length of approximately 50-500 nm. These plate-like nanostructures are found to be porous which is clearly visible in the high

magnification SEM image (Figure 4b). The presence of a small population of non-porous rod-like structures of Ga_2O_3 with width around 20-80 nm is also observed in the sample.

The morphological structure of α-Ga_2O_3 flakes was characterized further by TEM and high resolution TEM (HRTEM) imaging. Herein the existence of porous plate-like and non-porous rod-like structures of Ga_2O_3 nanoflakes could be confirmed (Figure 4c-d). The nature of the pores in the larger plates of Ga_2O_3 was investigated further using HRTEM, which revealed that these plates consist of crisscrossed rods which are placed out of registry, leading to pore formation (Figure 4d). The formation of these porous structures might be caused by dehydration and shrinking during the conversion process from GaOOH to Ga_2O_3.[3a, 18] The bottom two inset images of Figure 4c illustrate the SAED pattern and the lattice fringes for the synthesized nano particles. The right inset profile displays well-defined lattice fringes with the *d*-spacing of approximately 0.50 nm between two lattice planes, consistent with the unit cell dimension of hexagonal Ga_2O_3. The left inset exhibits the SAED image which provides the inter-planar spacing of 0.25 nm that is consistent with the *d*-spacing values of the (110) plane of hexagonal α-Ga_2O_3.[8a]

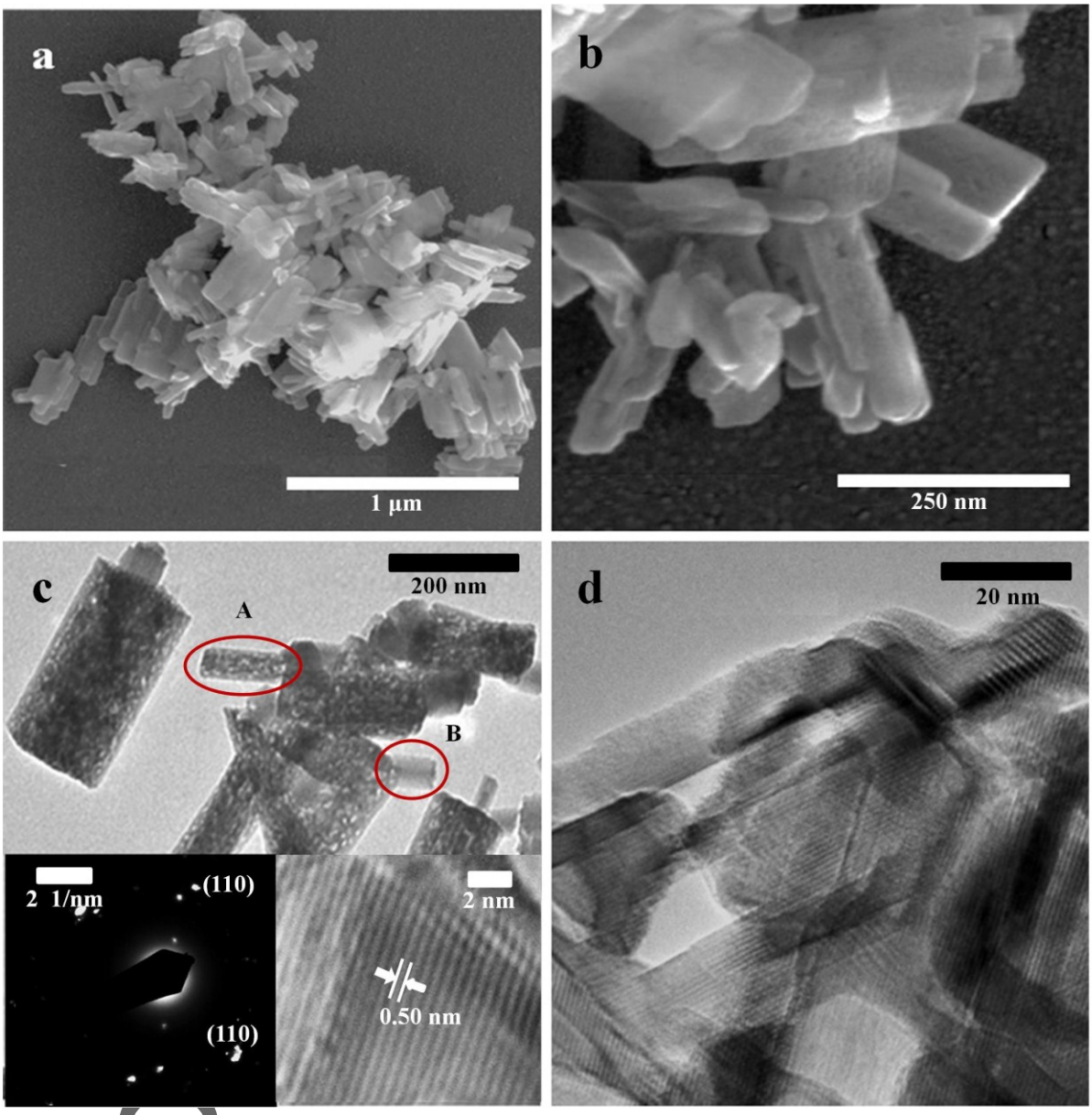

Figure 4. (a) SEM image of α-Ga_2O_3. (b) High-magnification SEM images of Ga_2O_3 nanoflakes. (c) TEM image of α-Ga_2O_3 indicating the flake like porous (A) and nonporous (B) populations as indicated. The insets show lattice fringes (bottom right inset) and SAED pattern (bottom left inset). (d) HRTEM micrograph of porous Ga_2O_3 flakes.

The chemical bonding states of the synthesized Ga_2O_3 were confirmed by XPS (Figure S2, Supporting Information). As shown in Figure S2, peaks at binding energy of 20.68 and 532.1 eV can be attributed to the valence state Ga 3d (Ga^{3+}) and O 1s in Ga_2O_3, respectively.[20] No metallic gallium (Ga^0) was observed in the Ga 3d region, confirming the efficiency of the oxidation process and the subsequent reaction workup. Furthermore, the characteristic oxygen and gallium peaks of GaOOH located at 530.8 and 19.8 eV, respectively, were not observed, evidencing quantitative dehydration.[21] The observed binding energies are all consistent with the previous reported values for Ga_2O_3.[20]

The surface morphology and thicknesses of the synthesized Ga_2O_3 nanoflakes were investigated using atomic force microscopy (AFM). The height profiles indicate that the nanostructures have a typical thickness of approximately 5 to 20 nm (a typical flake of 6 nm thick as presented in **Figure 5**). The pores are not resolved during AFM imaging, since their dimensions are smaller than the radius of the AFM tip, which defines the resolution of the technique. Considering the lengths, widths and thicknesses of the synthesized structures the obtained nanomaterial can be described as either quasi-one dimensional (nano-rods) or quasi-two dimensional (nano-plates or nano-flakes).

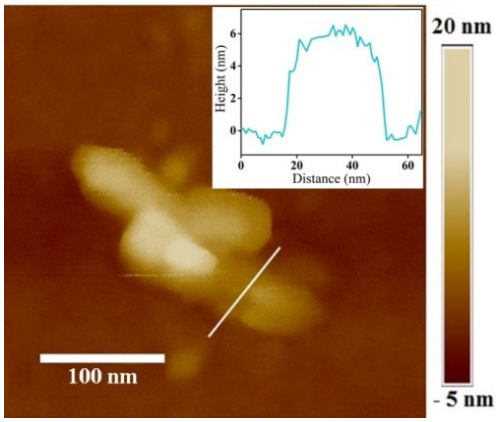

Figure 5. AFM image of α-Ga_2O_3 nanostructures. Inset: height profile along the white line.

The specific surface area and the corresponding pore size distribution of the Ga_2O_3 nanostructures were determined using the Brunauer–Emmett–Teller (BET) surface area and Barrett–Joyner–Halenda (BJH) pore size & volume analysis. The surface area of the prepared Ga_2O_3 was found to be 31.12 m^2/g. From the BJH method, the adsorption cumulative pore volume was found to be 0.042 cm^3/g. The trace of pore width was obtained to be 4 nm on average that demonstrates the nanoporous characteristics of the sample.

Optical properties of Ga_2O_3 samples were explored by UV–vis absorption spectroscopy, which is illustrated in **Figure 6**a-b. The spectrum of synthesized Ga_2O_3 shows strong absorption in the UV region (Figure 6a). Light absorption of α-Ga_2O_3 starts at around 260 nm which is consistent with previous reports.[8b] Further inspection reveals a relatively broad but weak absorption peak in the wavelength range between 280-400 nm, which may be caused by the presence of trap states in the band gap of the synthesized oxide. The direct band gap of α-Ga_2O_3 has been determined 4.65 eV using Tauc's analysis (Figure 6b) which is consistent with previous literatures.[3a, 11a, 12a, 22]

The other components of the electronic band structure of Ga_2O_3 were obtained using valence band XPS (VB-XPS) and photoemission spectroscopy in air (PESA). PESA analysis is usually conducted to determine work function of metals and the ionization potential (IP) of semiconductors. The IP of semiconductors may refer to either the valence band position or to trap states within the bandgap,

provided that their density is high enough to result in a detectable signal.[23] The PESA spectrum of Ga_2O_3 (Figure 6c) reveals an unusual two-step dependency instead of the commonly observed single emission edge. The ionization potential of the sample was determined to be −4.25 eV, with the second emission edge having an energy of approximately −5.0 eV. The unusual shape of the PESA spectrum is indicative of the presence of trap states, leading to the conclusion that the PESA signal originates from inter-bandgap states rather than electrons in the valence band. This assertion is confirmed further when the optical bandgap of the material is considered. If the emission edges observed in PESA were associated with the valence band, the conduction band edge would be placed close to or even above the vacuum level, which is obviously not possible. The observations are similar to reports on tin doped indium oxide, where the measured IP corresponds to the top of the dopant-associated trap band and the PESA signal corresponds to the Fermi level of the material.[23a]

VB XPS was employed to investigate the density of states (DOS) of the valence band area of α-Ga_2O_3 (Figure 6d). The VB XPS spectrum reveals that the difference between the valence band edge and the Fermi level is approximately 3 eV. It is noted that significant DOS intensity is present between the VB maximum and the Fermi level. This DOS is associated with the aforementioned trap states within the energy band gap. The presence of such trap bands in α-Ga_2O_3 has been previously reported and associated with oxygen and/or gallium vacancies.[11c, 11e, 24]

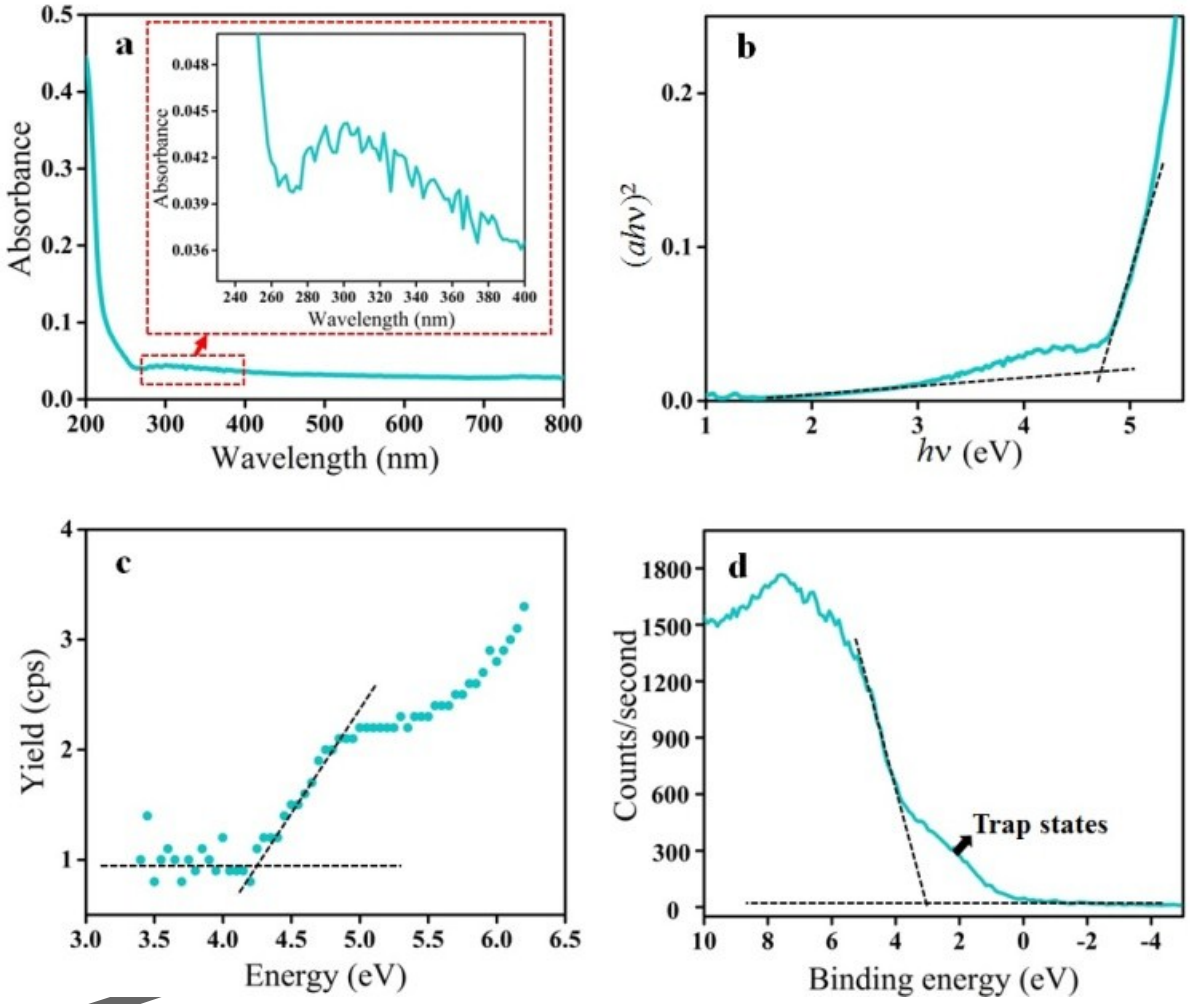

Figure 6. (a) UV-vis absorbance spectrum of α-Ga_2O_3 exhibiting a broad absorption feature between 280-400 nm. (b) Tauc-plot of the UV-vis data where plot *α* and *hν* represents the optical absorption coefficient and photon energy respectively. (c) PESA spectrum of α-Ga_2O_3. (d) VB XPS analysis showing the presence of trap states.

The photocatalytic performance of Ga_2O_3 was explored *via* the decomposition of the organic model compound Congo red (CR). CR was chosen as a suitable model dye due to its complex chemical structure and use in previous works on evaluating photocatalytic activities.[25] The gradual reduction of the characteristic absorbance spectrum for CR dye in the presence of the catalyst under solar light irradiation was monitored to evaluate the photocatalytic degradation performance. The concentration of a prepared resuspended α-Ga_2O_3 stock solution was measured to be 0.20 mg/ml using thermal gravimetric analysis (TGA).[26] Prior to solar irradiation, 1.65 ml of the suspended photocatalyst were added to 2 ml of 10 µM CR stock solution, leading to a reaction mixture containing 0.09 mg/ml of Ga_2O_3 and 4.5 µM CR. The solution was then illuminated with simulated AM1.5 1000 W m^{-2} solar light, which closely resembles the ambient solar spectrum. Photocatalytic dye degradation was performed for 120 min and the absorbance of the CR solution was measured in regular intervals (20 min) in order to determine the photodegradation rate.

The absorption spectra of the reaction mixture containing CR and suspended α-Ga_2O_3 nanoparticles, before and during photocatalysis, are presented in **Figure 7**a. It is evident that the characteristic absorption peak of CR centered at 500 nm degrades significantly and almost diminishes within 120 min. The breakdown of the chromophoric configuration of the target dye is confirmed by the steady color change of CR solution from an intense red-pink to almost colorless solution after 120 min of simulated solar light irradiation (inset of Figure 7a).

Figure 7b illustrates the relative absorbance change (A_t/A_0) and dye degradation percentage of CR, where A_0 is the initial absorbance of the dye without any irradiation and A_t is the absorbance of the dye at time (t). Three different conditions were considered for the investigation: (a) a blank experiment in the absence of solar light but in the presence of the photocatalyst, (b) a blank

experiment in the absence of photocatalyst but in the presence of the solar light and (c) experiment in the presence of both light and catalyst. In the presence of the catalyst and under illumination, it is observed that 70% of CR is eliminated after 60 min (Figure 7b). The reaction kinetics were found to be well described by a pseudo-first order reaction model.[27] To evaluate the nature of the degradation kinetics $ln\,(A_t/A_0)$ was plotted against irradiation time and the rate constant k was obtained as 0.0161 min^{-1} (Figure S3, Supporting Information). The blank experiment conducted without illumination revealed a negligible decrease of the dye's absorbance, which is likely associated with the adsorption of dye molecules to the surface of the catalyst. Overall, the observation of the dark experiment signifies the effective degradation of organic molecules by the catalyst (Figure S4, Supporting Information). Another blank experiment was conducted to observe the degradation of CR under solar irradiation without the presence of any photocatalyst. This control experiment confirmed that no degradation of CR occurred during the experimental timeframe of 120 min, confirming the activity of the photocatalyst (Figure S5, Supporting Information).

The photocatalytic activity of the synthesized Ga_2O_3 was further evaluated by investigating of Rhodamine B (RhB) dye degradation under solar light irradiation, while keeping the identical conditions including the photocatalyst loading and dye concentration that were used for the CR study. RhB shows a prominent absorption band at 554 nm and the absorbance decreased significantly under solar irradiation. The obtained results for RhB dye degradation are presented in Supporting Information (Figure S6 and S7). The results prove that Ga_2O_3 nanostructures can also effectively catalyze and degrade RhB dye confirming that Ga_2O_3 possess a general photocatalytic property. However, the photocatalytic activity of α-Ga_2O_3 is slightly higher for CR in comparison to RhB. It is seen that nearly 84% of RhB dye is eliminated after 120 min.

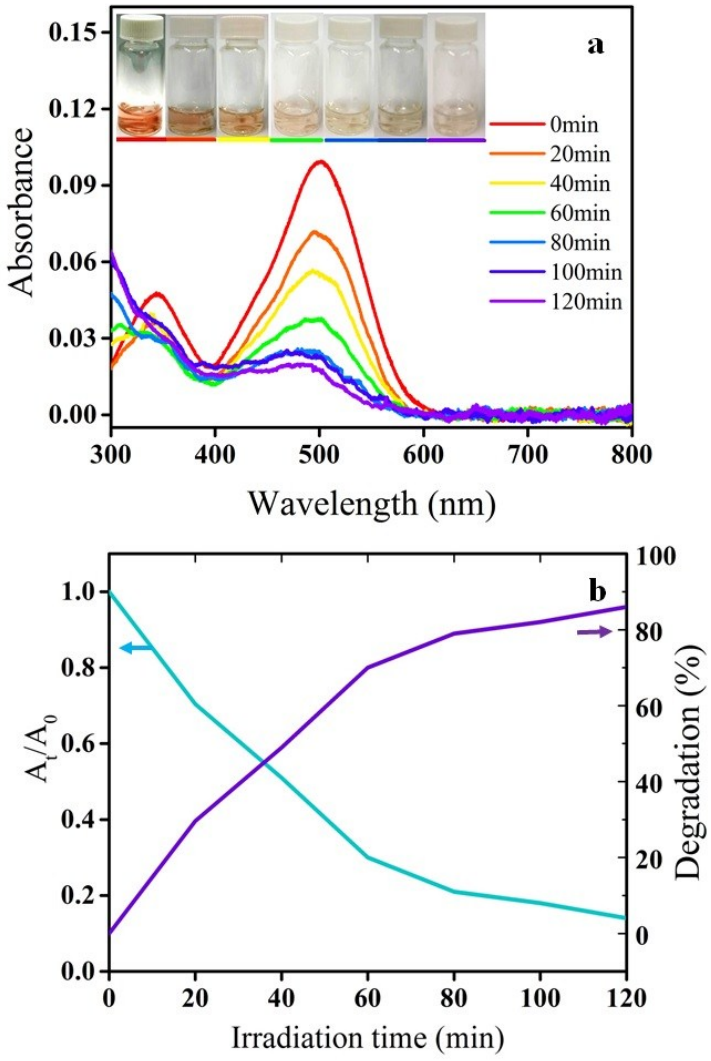

Figure 7. (a) UV-vis absorption spectra of CR in the presence of the Ga_2O_3 catalyst after indicated duration of simulated solar light irradiation. (b) Photodegradation of CR under solar light irradiation.

A comparison between the dye degradation performance observed in this work and a selection of previous reports on different phases of gallium oxide is presented in **Table 1**. A meaningful

comparison is only possible when considering different light sources used in the respective experimental setup. As can be seen in Table 1, most studies utilize high power UV irradiation leading to experimental conditions which are not representative of likely application scenarios. Furthermore, the use of high power UV irradiation leads to exaggerated dye-degradation rates when wide bandgap semiconductors such as Ga_2O_3 are investigated. Our experimental setup on the other hand utilizes a specially designed solar simulator that provides calibrated light with a spectrum that closely resembles solar radiation as it is naturally observed. Our developed photocatalyst outperforms all previous reports on Ga_2O_3 despite being tested in a realistic scenario where the near UV photon flux is likely orders of magnitude lower then where high power UV-lamps are used.

Table 1. Comparison of photocatalytic performance of a selection of previously reported gallium oxide and this work.

Material	Average width/ diameter	Dye concen-tration (mol/L)	Photo-catalyst concen-tration (mg/L)	Target dye	Illumination source	C/Co after 60 min	Dye degra-dation after 60 min	Kinetic rate constant, *K* (min^{-1})	Ref.
β-Ga_2O_3 nanorods	50 nm	2×10^{-5}	1000	RhB	150 W Xenon lamp*	~0.66	34%	~0.015	[1]
α-Ga_2O_3 nanorods	(50-100) nm	0.84×10^{-5}	1000	RhB	UV lamp*	~0.38	62%	-	[3a]
β-Ga_2O_3 nanobelts	~ (50-90) nm	1×10^{-5}	-	RhB	UV lamp*	~0.59	41%	0.0087	[11e]
β-Ga_2O_3	~(1-3) µm	2×10^{-5}	1000	RhB	150 W	~0.4	60%	-	[8b]

microspheres					Xenon lamp*				
β-Ga_2O_3 sheet	-	2.15×10^{-5}	500	CR	30W UV lamp*	~0.67	33%	0.005	[28]
β-Ga_2O_3 nanorods	(280-400) nm	2×10^{-4}	1000	RhB	100W UV lamp*	~0.62	38%	-	[29]
Floral β-Ga_2O_3 nanorods	~1μm	2×10^{-5}	1000	RhB	150W Xenon lamp*	~0.61	39%	-	[12b]
α-Ga_2O_3 nanoplates	(25-250) nm	0.45×10^{-5}	90	CR	AM1.5 1000 W m^{-2} solar simulator	0.30	70%	0.016	This work
α-Ga_2O_3 nanoplates	(25-250) nm	0.45×10^{-5}	90	RhB	AM1.5 1000 W m^{-2} solar simulator	0.47	53%	0.014	This work

* Energy per surface area has not been provided

The significant improvement in photocatalytic activity of the synthesized Ga_2O_3 can be attributed to two distinct phenomena: (1) the high porosity of the plates and rods that offer a large surface to volume ratio nanostructure for enhancing photocatalytic activity but more importantly (2) the modified energy band structure of the synthesized Ga_2O_3 due to the presence of trap states. An energy band diagram for the synthesized Ga_2O_3 is proposed in **Figure 8**, based on UV-vis spectroscopy, VB XPS and PESA analysis (Figure 6c-d). These characterizations revealed that the edge of the aforementioned trap band, which constitutes an extension of the valence band, is located at approximately −4.25 eV. Considering the VB XPS results that indicate a depth of 3.0 eV of the trap

band, the valence band edge is situated at −7.25 eV (Figure 8). Based on the measured direct optical bandgap of 4.65 eV, we expect the conduction band minimum (CBM) to be situated at −2.60 eV. As discussed before, the broadening of the valance band width is ascribed to the generation of trap states (marked as a grey line in Figure 8). Therefore, the band gap of Ga_2O_3 is significantly decreased, leading to the expansion of photocatalytic activity into the visible-light range (Figure 8). Upon solar light irradiation, the excited electrons of Ga_2O_3 in trap states are promoted to the conduction band. The conduction band position is estimated at highly reducing potentials providing ample driving force for subsequent reactions. Therefore, these photo-generated electrons effectively produce superoxide radicals ($O_2^{-\bullet}$) through subsequent reduction reactions. Eventually, these superoxide radicals play a significant role for decomposing the organic dye CR.[30] In order to fully elucidate possible dye-photocatalyst interactions, we determined the highest occupied molecular orbital (HOMO) and the corresponding lowest unoccupied molecular orbital (LUMO) energies for both investigated dyes. The HOMO level of organic chromophores can be estimated by measuring their ionization potentials using PESA, the corresponding LUMO level can be obtained when the optical gap of the chromophore is considered.[31] The energy levels of CR dye which have been previously reported as - 5.26 eV and -2.48 eV for HOMO and LUMO, respectively, are shown in Figure 8.[25] Considering the LUMO position of CR, there is a small driving force for electron injection into the conduction band of Ga_2O_3 (-2.60 eV) as shown in Figure 8.[32] As a result CR might engage in dye-sensitization of Ga_2O_3, providing additional charge carriers that may be available for the photocatalytic reaction. The HOMO level of RhB is found -5.32 eV using PESA (Figure S8, Supporting Information). Consequently, the LUMO level can be calculated -2.47 eV using the energy level difference of RhB dye.[33]

Overall, it can be concluded that the enhanced photocatalytic performance is influenced by the reduced bandgap due to presence of trap states, which allow efficient light harvesting while maintaining a conduction band edge that is highly reducing.

The existence of trap states is further investigated by conducting the photoluminescence (PL) analysis of the synthesized Ga_2O_3 suspension. Figure 8 b presents the PL spectrum of the Ga_2O_3 sample in an aqueous solution excited at 500 nm. A relatively broad emission peak is observed in the range of 625 to 730 nm, which corresponds to the bandgap energy of 2.0 to 1.7 eV. These emissions are consistent with the estimated bandgap values in our study and seem to be originated from the trap states located in their upper valance band area.

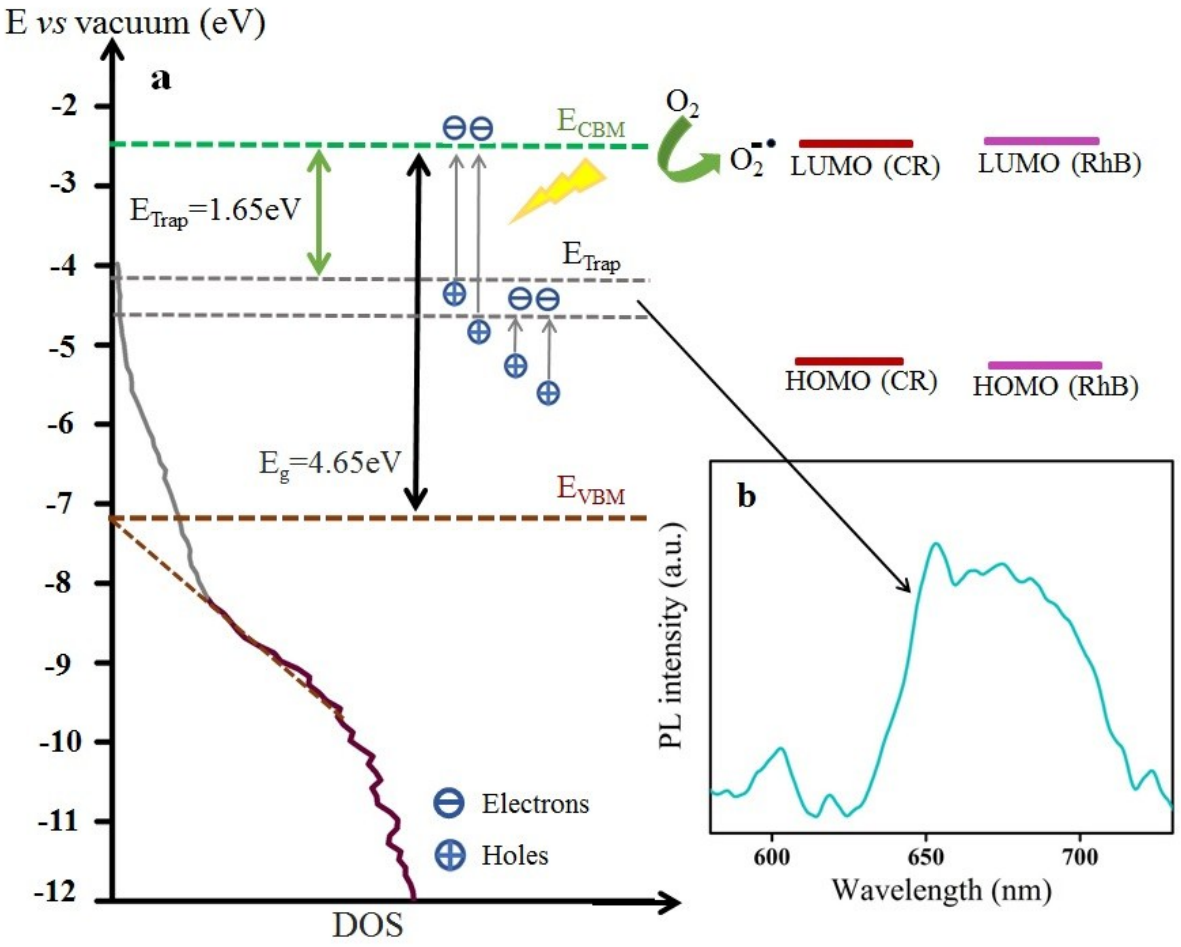

Figure 8. (a) Energy level diagram of Ga_2O_3 representing the possible photocatalytic mechanism with the estimated valance band maximum (VBM) and CBM. The DOS was determined by VB XPS. HOMO and LUMO values for CR and RhB are also demonstrated. (b) Room temperature PL spectrum of α-Ga_2O_3 in solvent.

In order to assess whether the trap states are associated with surface defects or bulk dislocations, PL of the material was obtained before and after etching the surface of Ga_2O_3 using oxygen plasma. These measurements were carried out in ambient air (drop-casted on SiO_2 substrates) and as such

the side tails are significantly more stretched around the center peak in comparison to the in liquid PL measurement. **Figure 9** shows the change in PL spectrum of Ga_2O_3 after plasma etching treatment. The Ga_2O_3 samples were subjected to 3 successive 3 seconds of plasma treatment at 60 W. It is observed that the intensity of the obtained PL peaks have decreased with increasing the etching time. This indicates that trap states, responsible for the reduction of bandgap energy and PL emission (Figure 8), are mostly located on the surface rather than bulk. It is also noticed that in air all PL spectra have significant low-energy tails. These PL tails are possibly originated from the intra-band transitions between the defect states (Figure 8).

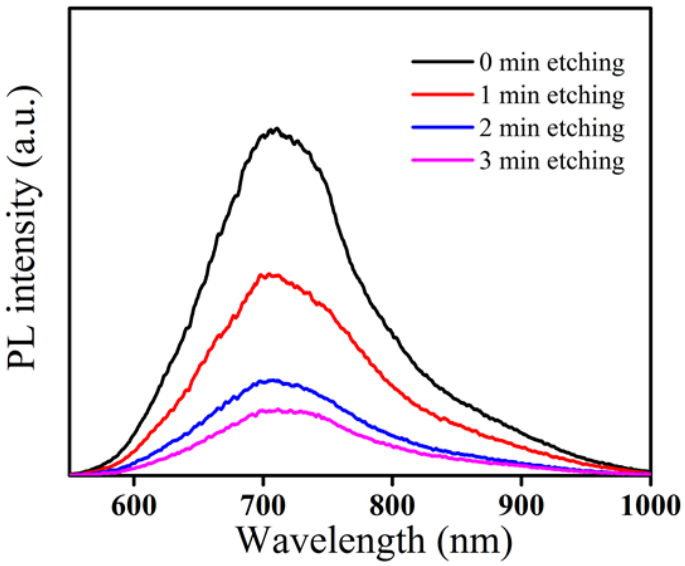

Figure 9. Room temperature PL spectra of α -Ga_2O_3 in air obtained at the excitation wavelength of 532 nm.

3. Conclusion

In summary, a new method for synthesizing high surface-to-volume ratio porous plates and rods α-Ga_2O_3 from liquid metal gallium was demonstrated. We introduced a facile two-step method to synthesize Ga_2O_3 nanostructures from bulk liquid metal gallium *via* sonication and subsequent annealing to produce first gallium oxy-hydroxide and then gallium oxide nanostructures. The morphological, structural and optical properties of the synthesized nanoparticles were thoroughly investigated, leading to the conclusion that the synthesized material was hexagonal α-Ga_2O_3 nanoflakes with high porosity. As an application, the photocatalytic activity of the synthesized oxide nanoparticles was investigated for degrading CR and RhB dyes under solar light irradiation, which exhibited a remarkable performance, reaching dye degradation of 70% in 60 min under a solar sun simulator (outcome of RhB dye is also demonstrated). The mechanism behind the efficient photocatalytic performance of Ga_2O_3 was investigated and an energy band diagram was established utilizing PESA, valance band XPS and UV–vis analysis. On the basis of the developed energy level diagram, it was concluded that the enhanced photocatalytic performance originated from a narrowed band gap of 1.65 eV caused by the raised valance band, induced by trap states. As such, we report a promising method for developing effective solar light gallium oxide photocatalysts at high yield following a facile and inexpensive synthesis route enabling practical future electronic and optical applications.

4. Experimental Section

***Two step liquid metal based Ga_2O_3 synthesis*:** A bath sonication method was adopted to synthesize gallium oxide nanoparticles using gallium metal as the precursor and DI water as both the reaction medium and oxygen source. The synthesis of gallium oxide flakes involves a two-step process. In the first step, a suspension of hydrated gallium oxide nanoparticles was produced by sonicating bulk liquid gallium in DI water at 50°C. During this step 900 mg of gallium (0.15 ml) were added to 15 ml DI water. The liquid was sealed in a sample vial and sonicated in a bath sonicator for 60 min. The experimental design was influenced by our previous observation indicating that 60 min is sufficient to transform the majority of the bulk metal into solid nanoparticles with only few liquid metal droplets remaining in suspension.[20] The obtained suspension was then centrifuged for 15 min at 100 RCF (Eppendorf Centrifuge 5702) to remove residual gallium metal and large oxide particles. The supernatant containing hydrated gallium oxide nanoparticles was collected and dried in an electric furnace for around 45 min at 120°C.

In the second step, the dried hydrated gallium oxide nanoparticles were heated in an electric furnace at 450°C for 4 h in air using a heating rate of 10 °C/min in the beginning of the procedure (total time 280 min). The gallium oxide flakes were then re-suspended in 6 ml of DI water. Sonication in a bath sonicator for 10 min for the final re-suspension was found to be sufficient to achieve a homogeneous suspension.

***Characterizations*:** To determine the crystallinity and phase purity of the synthesized material, XRD patterns were obtained using a Bruker D4 Endeavour featuring a CuKα X-ray source (λ=1.54 Å). The nanoparticle morphology, crystal structure and lattice properties were evaluated further by TEM (JEOL 1010) and HRTEM (JEOL 2010F) at acceleration voltages of 100 and 200 kV, respectively. SAED patterns were obtained using the JEOL 2010F microscope. XPS (Thermo Scientific K-Alpha X-ray

Spectrophotometer) was utilized to assess the materials' composition and to collect the valence band spectrum. Absorbance measurements were performed using an Agilent Cary 60 Ultraviolet-Visible Spectrophotometer. SEM (FEI Scios Dualbeam FIBSEM) was used for exploring the morphological properties. The surface thickness and roughness of the synthesized materials were assessed using a Bruker Dimension Icon AFM. To study the valence band energy levels, PESA (Riken Keiki AC-2) was utilized at a power of 500 nW. The amount of weight variation of the material, as a function of increasing temperature and time, were evaluated by TGA (Perkin Elmer Pyris 1) in an atmosphere of nitrogen gas, providing a measure of the oxide loading in liquid suspension. The photocatalytic performance was evaluated using a Sol3A class AAA solar simulator IEC/JIS/ASTM equipped with a 450W Xenon lamp. The power was adjusted to precisely 1 sun (AM1.5) using a Silicon reference cell accredited by NIST to the ISO-17025 standard. PL spectrum of Ga_2O_3 nanostructures in solvent was collected using a PerkinElmer LS50 luminescence spectrometer with an excitation wavelength of 500 nm. PL measurements of Ga_2O_3 in air were conducted using Horiba Scientific LabRAM HR evolution Raman/PL spectrometer. Solarus (Model 950) Advanced Plasma Cleaning System was used for plasma treatment. The surface properties (surface area, pore size, and pore volume) were measured with the aid of *Micromeritics ASAP* 2400 instrument.

Supporting Information

Supporting Information on additional TEM, SEM, XPS, PESA and more photocatalysis details are available from the Wiley Online Library or from the author.

Acknowledgements

We thank the scientific and technical assistance of the RMIT Microscopy and Microanalysis Facility (RMMF) and the RMIT Micro Nano Research Facility (MNRF). The authors would also like to thank the Australian Research Council (ARC) that supported this project under the Discovery Project DP170102138.

5. References

[1] K. Girija, S. Thirumalairajan, A. K. Patra, D. Mangalaraj, N. Ponpandian, C. Viswanathan, *Semicond. Sci. Technol.* **2013**, 28, 035015.

[2] a) M. Muruganandham, R. Amutha, M. S. A. Wahed, B. Ahmmad, Y. Kuroda, R. P. Suri, J. J. Wu, M. E. Sillanpaa, *J. Phys. Chem. C* **2011**, 116, 44; b) H.-S. Qian, P. Gunawan, Y.-X. Zhang, G.-F. Lin, J.-W. Zheng, R. Xu, *Cryst. Growth Des.* **2008**, 8, 1282.

[3] a) D. Li, X. Duan, H. Fan, W. Zheng, *J. Mater. Chem. A* **2013**, 1, 12417; b) Y. Lu, Q. Hu, Y. Lin, D. B. Pacardo, C. Wang, W. Sun, F. S. Ligler, M. D. Dickey, Z. Gu, *Nat. Commun.* **2015**, 6, 10066.

[4] a) G. Guzman-Navarro, M. Herrera-Zaldivar, J. Valenzuela-Benavides, D. Maestre, *J. Appl. Phys.* **2011**, 110, 034315; b) C. Liang, G. Meng, G. Wang, Y. Wang, L. Zhang, S. Zhang, *Appl. Phys. Lett.* **2001**, 78, 3202.

[5] W. S. Hwang, A. Verma, H. Peelaers, V. Protasenko, S. Rouvimov, H. Xing, A. Seabaugh, W. Haensch, C. Van de Walle, Z. Galazka, M. Albrecht, R. Fornari, D. Jena, *Appl. Phys. Lett.* **2014**, 104, 203111.

[6] T. Minami, Y. Nishi, T. Miyata, *Appl. Phys. Express* **2013**, 6, 044101.

[7] a) Y. Li, A. Trinchi, W. Wlodarski, K. Galatsis, K. Kalantar-zadeh, *Sens. Actuators B Chem.* **2003**, 93, 431; b) M. Ogita, K. Higo, Y. Nakanishi, Y. Hatanaka, *Appl. Surf. Sci.* **2001**, 175, 721.

[8] a) X. Wang, Q. Xu, M. Li, S. Shen, X. Wang, Y. Wang, Z. Feng, J. Shi, H. Han, C. Li, *Angew. Chem. Int. Ed.* **2012**, 51, 13089; b) K. Girija, S. Thirumalairajan, V. R. Mastelaro, D. Mangalaraj, *J. Mater. Chem. A* **2015**, 3, 2617.

[9] a) A. Mills, R. H. Davies, D. Worsley, *Chem. Soc. Rev.* **1993**, 22, 417; b) Z. Zou, J. Ye, K. Sayama, H. Arakawa, *Nature* **2001**, 414, 625; c) A. Gautam, A. Kshirsagar, R. Biswas, S. Banerjee, P. K. Khanna, *RSC Adv.* **2016**, 6, 2746; d) E. Wang, P. Zhang, Y. Chen, Z. Liu, T. He, Y. Cao, *J. Mater. Chem.* **2012**, 22, 14443; e) J. Kim, C. W. Lee, W. Choi, *Environ. Sci. Technol.* **2010**, 44, 6849.

[10] H. Dong, G. Zeng, L. Tang, C. Fan, C. Zhang, X. He, Y. He, *Water Res.* **2015**, 79, 128.

[11] a) Y. Hou, X. Wang, L. Wu, Z. Ding, X. Fu, *Environ. Sci. Technol.* **2006**, 40, 5799; b) H.-a. Park, J. H. Choi, K. M. Choi, D. K. Lee, J. K. Kang, *J. Mater. Chem.* **2012**, 22, 5304; c) W. Zhang, B. S. Naidu, J. Z. Ou, A. P. O'Mullane, A. F. Chrimes, B. J. Carey, Y. Wang, S.-Y. Tang, V. Sivan, A. Mitchell, S. K. Bhargava, K. Kalantar-zadeh, *ACS Appl. Mater. Interfaces* **2015**, 7, 1943; d) X.

Li, X. Zhen, S. Meng, J. Xian, Y. Shao, X. Fu, D. Li, *Environ. Sci. Technol.* **2013**, 47, 9911; e) L. C. Tien, W. T. Chen, C. H. Ho, *J. Am. Ceram. Soc.* **2011**, 94, 3117.

[12] a) Y. Hou, L. Wu, X. Wang, Z. Ding, Z. Li, X. Fu, *J. Catal.* **2007**, 250, 12; b) K. Girija, S. Thirumalairajan, A. K. Patra, D. Mangalaraj, N. Ponpandian, C. Viswanathan, *Curr. Appl. Phys* **2013**, 13, 652.

[13] a) M. Nolan, *ACS Appl. Mater. Interfaces* **2012**, 4, 5863; b) M. Bagheri, A. R. Mahjoub, A. A. Khodadadi, Y. Mortazavi, *RSC Adv.* **2014**, 4, 33262.

[14] a) R. Binions, C. J. Carmalt, I. P. Parkin, K. F. Pratt, G. A. Shaw, *Chem. Mater.* **2004**, 16, 2489; b) G.-S. Park, W.-B. Choi, J.-M. Kim, Y. C. Choi, Y. H. Lee, C.-B. Lim, *J. Cryst. Growth* **2000**, 220, 494; c) J. Hu, Q. Li, X. Meng, C. Lee, S. Lee, *J. Phys. Chem. B* **2002**, 106, 9536; d) G. Sinha, K. Adhikary, S. Chaudhuri, *Opt. Mater.* **2007**, 29, 718; e) M. Ristić, S. Popović, S. Musić, *Mater. Lett.* **2005**, 59, 1227; f) B. Geng, L. Zhang, G. Meng, T. Xie, X. Peng, Y. Lin, *J. Cryst. Growth* **2003**, 259, 291.

[15] a) Y. Hou, J. Zhang, Z. Ding, L. Wu, *Powder Technol.* **2010**, 203, 440; b) J. Zhang, Z. Liu, C. Lin, J. Lin, *J. Crys. Growth* **2005**, 280, 99; c) S. Fujihara, Y. Shibata, E. Hosono, *J. Electrochem. Soc.* **2005**, 152, C764; d) Y. Quan, D. Fang, X. Zhang, S. Liu, K. Huang, *Mater. Chem. Phys.* **2010**, 121, 142; e) C. R. Patra, Y. Mastai, A. Gedanken, *J. Nanopart. Res.* **2004**, 6, 509; f) X. Liu, G. Qiu, Y. Zhao, N. Zhang, R. Yi, *J. Alloy Compd.* **2007**, 439, 275.

[16] a) B. J. Carey, J. Z. Ou, R. M. Clark, K. J. Berean, A. Zavabeti, A. S. Chesman, S. P. Russo, D. W. Lau, Z.-Q. Xu, Q. Bao, O. Kavehei, B. C. Gibson, M. D. Dickey, R. B. Kaner, T. Daeneke, K. Kalantar-zadeh, *Nat. Commun.* **2017**, 8, 14482; b) Y. D. Kim, J. Hone, *Nature* **2017**, 544, 167.

[17] M. D. Dickey, *ACS Appl. Mater. Interfaces* **2014**, 6, 18369.

[18] S. Yan, L. Wan, Z. Li, Y. Zhou, Z. Zou, *Chem. Comm.* **2010**, 46, 6388.

[19] X. Liu, G. Qiu, Y. Zhao, N. Zhang, R. Yi, *J. Alloys Compd.* **2007**, 439, 275.

[20] W. Zhang, J. Z. Ou, S. Y. Tang, V. Sivan, D. D. Yao, K. Latham, K. Khoshmanesh, A. Mitchell, A. P. O'Mullane, K. Kalantar-zadeh, *Adv. Funct. Mater.* **2014**, 24, 3799.

[21] J. Epp, J. G. Dillard, A. Siochi, R. Zallen, S. Sen, L. Burton, *Chem. Mater.* **1990**, 2, 173.

[22] S. R. Thomas, G. Adamopoulos, Y.-H. Lin, H. Faber, L. Sygellou, E. Stratakis, N. Pliatsikas, P. A. Patsalas, T. D. Anthopoulos, *Appl Phys Lett* **2014**, 105, 092105.

[23] a) Z. Yu, I. R. Perera, T. Daeneke, S. Makuta, Y. Tachibana, J. J. Jasieniak, A. Mishra, P. Bäuerle, L. Spiccia, U. Bach, *NPG Asia Mater.* **2016**, 8, e305; b) R. J. Davis, M. T. Lloyd, S. R. Ferreira, M. J. Bruzek, S. E. Watkins, L. Lindell, P. Sehati, M. Fahlman, J. E. Anthony, J. W. Hsu, *J. Mater. Chem.* **2011**, 21, 1721.

[24] J. Zhang, F. Jiang, L. Zhang, *Phys. Lett. A* **2004**, 322, 363.

[25] P. Atkin, T. Daeneke, Y. Wang, B. Carey, K. Berean, R. Clark, J. Ou, A. Trinchi, I. Cole, K. Kalantar-zadeh, *J. Mater. Chem. A* **2016**, 4, 13563.

[26] M. M. aAlsaif, M. R. Field, T. Daeneke, A. F. Chrimes, W. Zhang, B. J. Carey, K. J. Berean, S. Walia, J. van Embden, B. Zhang, K. Latham, K. Kalantar-zadeh, J. Z. Ou, *ACS Appl. Mater. Interfaces* **2016**, 8, 3482.

[27] A. Olad, S. Behboudi, A. A. Entezami, *Bull. Mater. Sci* **2012**, 35, 801.

[28] M. Bagheri, A. R. Mahjoub, *RSC Adv.* **2016**, 6, 87555.

[29] L. S. Reddy, Y. H. Ko, J. S. Yu, *Nanoscale Res. Lett.* **2015**, 10, 364.

[30] D. Channei, B. Inceesungvorn, N. Wetchakun, S. Ukritnukun, A. Nattestad, J. Chen, S. Phanichphant, *Sci. Rep.* **2014**, 4, 5757.

[31] B. E. Hardin, A. Sellinger, T. Moehl, R. Humphry-Baker, J.-E. Moser, P. Wang, S. M. Zakeeruddin, M. Grätzel, M. D. McGehee, *J. Am. Chem. Soc* **2011**, 133, 10662.

[32] A. Hagfeldt, G. Boschloo, L. Sun, L. Kloo, H. Pettersson, *Chem. Rev* **2010**, 110, 6595.

[33] Y. Y. Lee, J. H. Moon, Y. S. Choi, G. O. Park, M. Jin, L. Y. Jin, D. Li, J. Y. Lee, S. U. Son, J. M. Kim, *J. Phys. Chem. C* **2017**, 121, 5137.

ToC

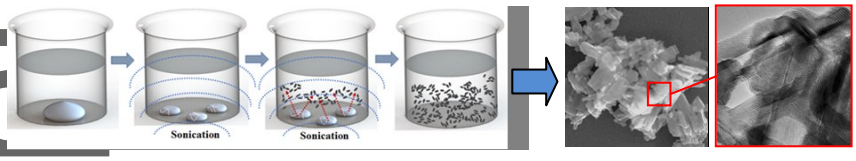

Sonication assisted route employed on liquid metal gallium has presented as a new route for synthesizing Ga_2O_3 nanoflakes. The suspension of Ga_2O_3 is used for dye degradation, showing a remarkable efficiency, which is ascribed to the presence of trap bands.

Supporting Information

Sonication Assisted Synthesis of Gallium Oxide Suspensions Featuring Trap State Absorption: Test of Photochemistry

*Nitu Syed, Ali Zavabeti, Md Mohiuddin, Baoyue Zhang, Yichao Wang, Robi S. Datta, Paul Atkin, Benjamin J. Carey, Cheng Tan, Joel van Embden, Anthony S. R. Chesman , Jian Zhen Ou, Torben Daeneke, Kourosh Kalantar-zadeh**

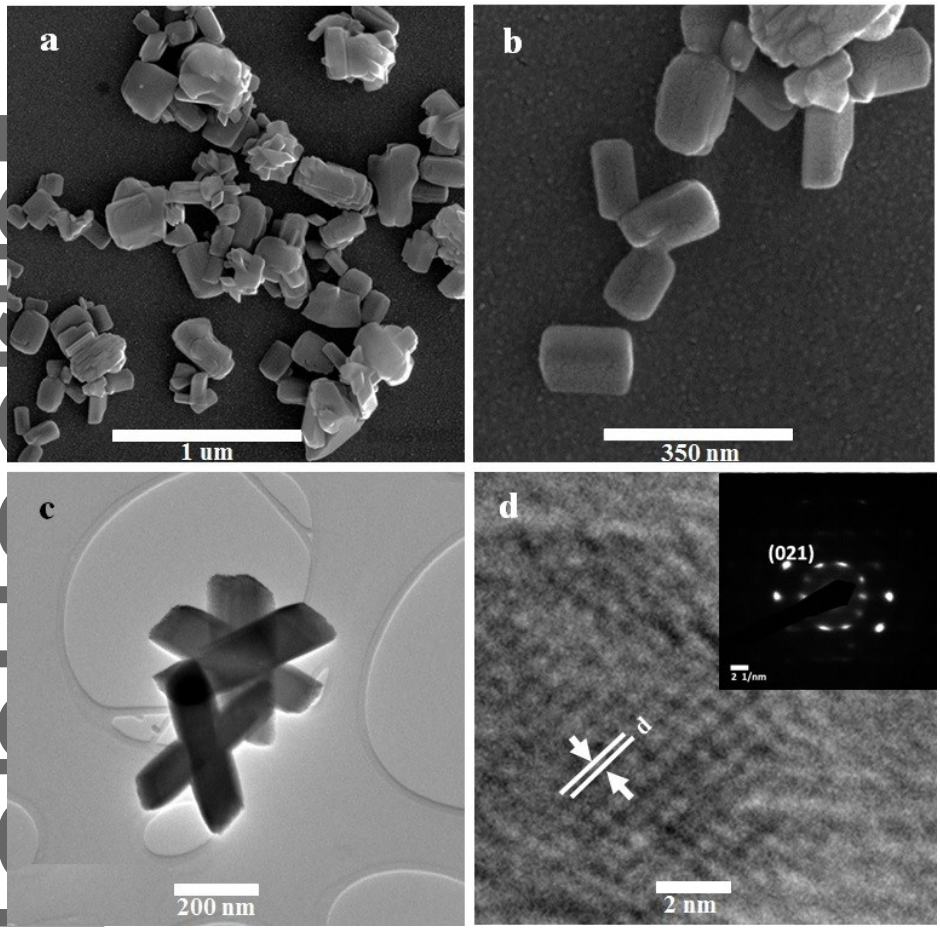

Figure S1. (a) SEM image of the GaOOH (b) High-magnification SEM image of the GaOOH nanoblocks. (c) The TEM image of the GaOOH, presenting plate-like structures. (d) HRTEM of GaOOH, displaying the lattice fringes. The top right inset of Figure S1(d) shows the SAED pattern of GaOOH, which indicates the observed interplanar spacing is 0.25 nm that corresponds to the *d*-spacing of (021) plane for orthorhombic GaOOH.[1]

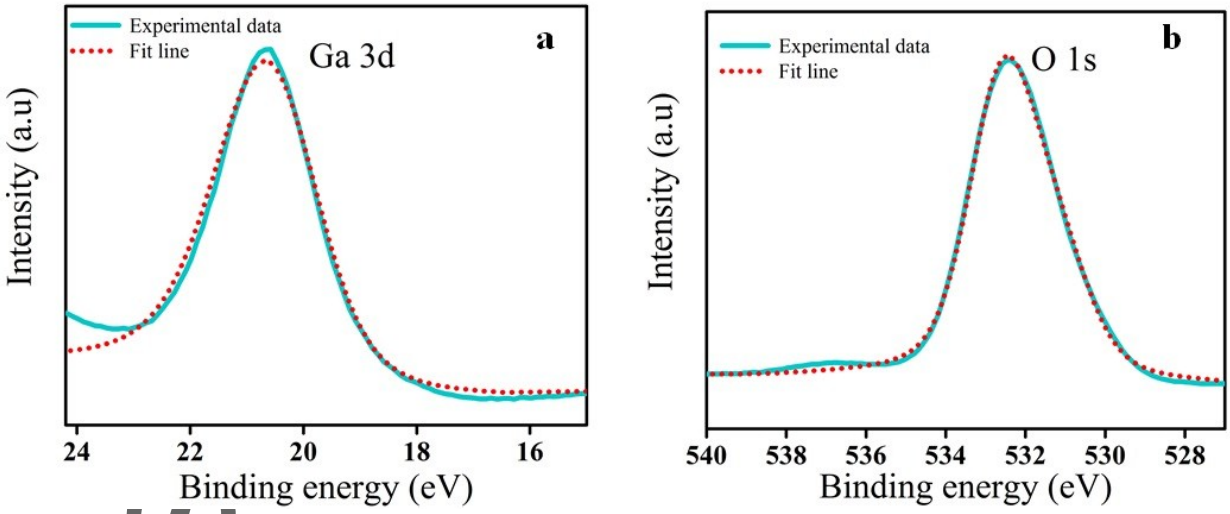

Figure S2. XPS of synthesized Ga_2O_3 (a) Ga 3d and (b) O 2s. Peak at the binding energy of 20.68 eV signifies the valence state Ga^{3+} in Ga_2O_3.[20] No metallic gallium (Ga^0) is observed in the Ga 3d region. Peak observed at a binding energy of 532.1 eV corresponds to O 1s state of Ga_2O_3.[2]

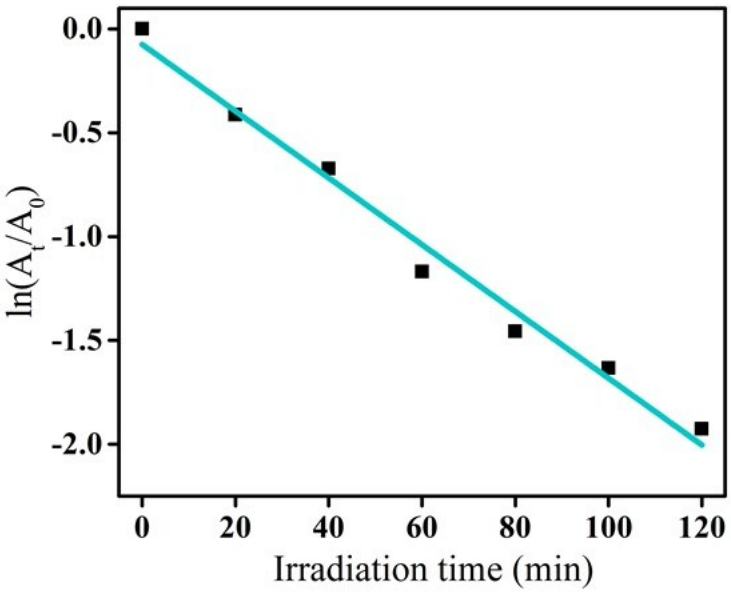

Figure S3. Degradation kinetics of Congo red dye under solar light irradiation where the slope is found to be 0.0161 min^{-1}.

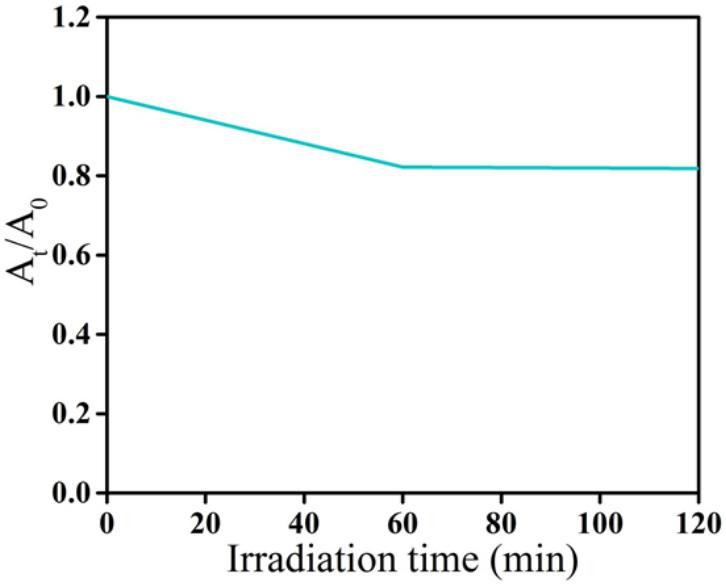

Figure S4. Degradation of Congo red in the presence of photocatalyst but in the absence of solar irradiation.

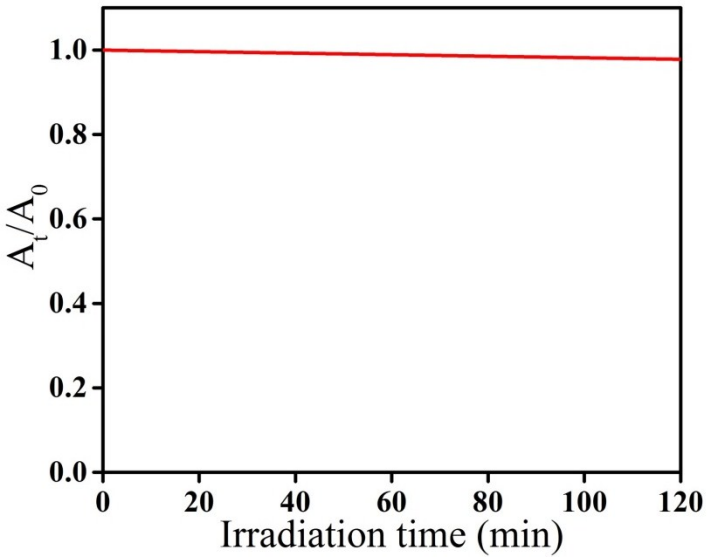

Figure S5. Degradation of Congo red under solar light irradiation without any photocatalyst.

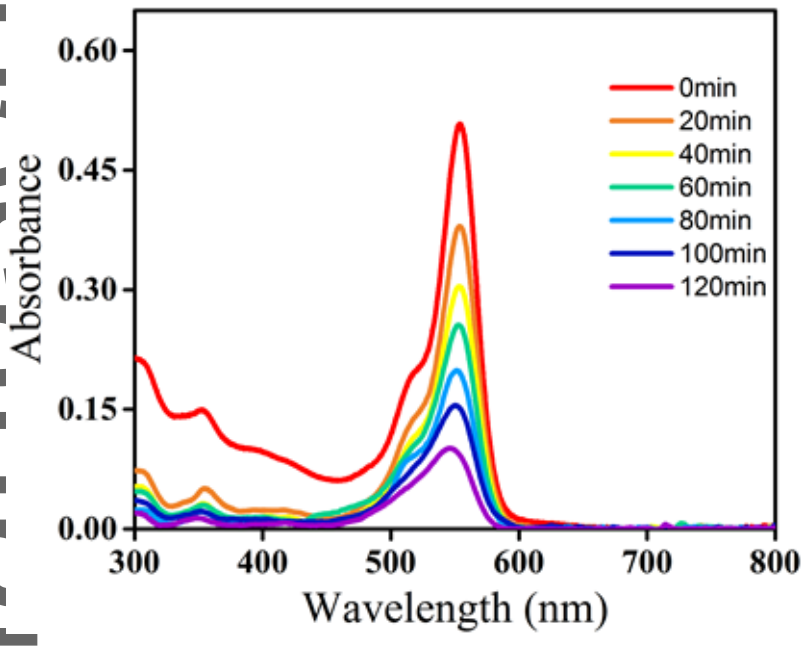

Figure S6. UV-vis absorption spectra of RhB in the presence of the Ga_2O_3 catalyst after the indicated duration of simulated solar light irradiation.

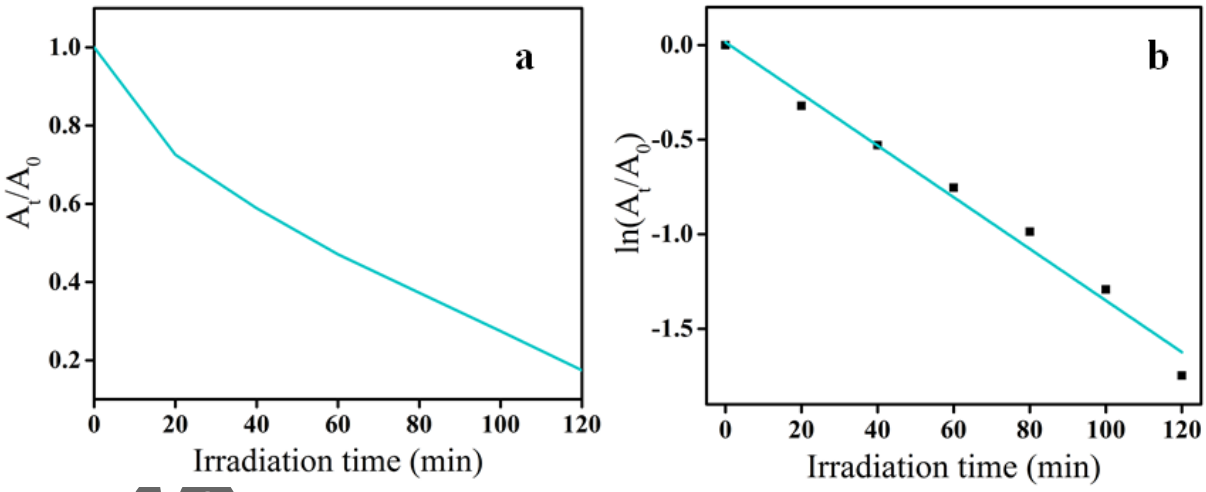

Figure S7. (a) Dye degradation rate of RhB under solar light irradiation. (b) Degradation kinetics of RhB show a slope 0.014 min^{-1}.

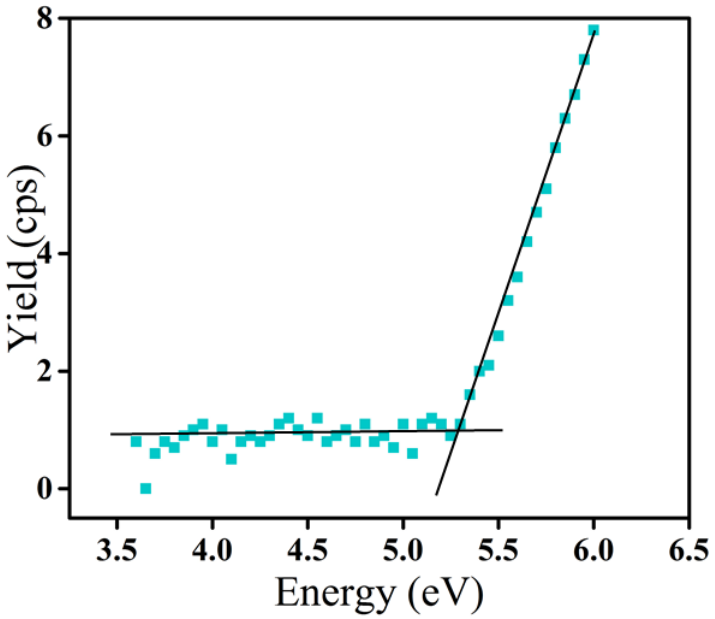

Figure S8. PESA spectrum of RhB indicating the HOMO level at -5.32 eV.

References

[1] L. Shi, J. Zhang, S. Wu, Y. Li, L. Jiang, Q. Cui, *J. Am. Ceram. Soc.* **2014**, 97, 2607.

[2] W. Zhang, J. Z. Ou, S. Y. Tang, V. Sivan, D. D. Yao, K. Latham, K. Khoshmanesh, A. Mitchell, A. P. O'Mullane, K. Kalantar-zadeh, *Adv. Funct. Mater.* **2014**, 24, 3799